Effects of sulphur on a Co/Mn based catalyst for Fischer-Tropsch reactions

Bjørn Christian Enger[1,*], John Walmsley[1,3], Ingeborg-Helene Svenum[1], Julian Richard Tolchard[1], Jia Yang[1,4], Rune Myrstad[1], Torbjørn Gjervan[1], Asad Ahmad Khan[2], Abdulkarim Mutairi-Al[2], Khalid Karim[2]

[1]SINTEF Industry, Postboks 4760 Sluppen, N-7465 Trondheim, Norway. [2]SABIC Technology and Innovation Centre, P.O. 42503, Riyadh-11551, Saudi Arabia. [3]Department of Materials Science and Metallurgy University of Cambridge, 27 Charles Babbage Road, Cambridge CB3 0FS, UK, [4]Department of Chemical Engineering, Norwegian University of Science and Technology, Sem Sælands vei 4, N-7491 Trondheim, Norway

* Corresponding author: bjorn.christian.enger@sintef.no

Abstract

The long term effect of up to 10 ppm H_2S was studied for Fischer-Tropsch conversion of syngas by catalytic testing at 240 °C, 5 bar, H_2/CO = 2.1 and GHSV = 2400 Nml/g,h. Sulphur was dosed after ~300 h or ~1000 h time on stream and the effect was monitored using on-line GC. The activity declined, and the effect correlated to the concentration of H_2S in the feed. However, dosing after ~1000 h caused a stronger effect than dosing after ~300 h. The effects of sulphur are significant with respect to operational risks and mitigation but are substantially less severe than for a standard Co-based catalyst operated at 20 bar for wax production. The spent catalyst consisted of a mixture of cubic (Co,Mn)O, hexagonal Co, Co_2C and sulphurous deposits; mainly $MnSO_4$. It could not be concluded that sulphur had a direct effect on product selectivity, but it may have impacted water-gas-shift activity, and sudden changes in shift activity was found to correlate to changes in hydrocarbon selectivity.

Keywords: Cobalt; Manganese; Fischer-Tropsch; syngas; sulphur; deactivation

1 Introduction

Sulphur is a compound found in natural gas, coal and biomass. It is a well-known poison for Fischer-Tropsch synthesis (FTS) catalysts [1, 2], and there are numerous reports on it's effects on cobalt based catalysts [1-16]. In fact, all catalysts that may be used in the synthesis of higher hydrocarbons from hydrogen and CO are readily poisoned by sulphur, and it is well established that there is a difference with respect to the effect of various sulphur compounds. For example, it is reported that CS_2 has a much stronger effect than H_2S [2]. An even more potent poison may be $(CH_3)_2S$ which reportedly causes 6 times faster deactivation compared to H_2S during *in-situ* poisoning. The effect was ascribed by the authors to more efficient site blocking due to the larger size of un-dissociated $(CH_3)_2S$ compared to dissociated H_2S [3]. In neither of these tests was there a direct effect of sulphur on selectivity evaluated beyond that expected from the changed CO conversion at elevated pressures [3].

It is commonly reported that sulphur compounds are not released in the outlet stream [1] and that the deactivation is permanent for Co catalysts, while adsorption is partly reversible on Ni and Ru catalysts depending on H_2S/H_2 ratio [1]. Interestingly there may also be a threshold on Co catalysts below which the presence of sulphur has little effect on the activity and one study in a CSTR has suggested a threshold at about 500 ppb [11]. This is an important finding as it was noted by the authors that such tolerance could allow for using a syngas that contains more sulphur than the 10 ppb that can be obtained by the Rectisol cleaning process. Although not directly comparable, model studies [13] of Co(0001) have demonstrated the formation of a sulphide and that the poisoned stated of Co FTS catalysts is a fully covered surface, corresponding to a nonselective poisoning mechanism.

There are two basic reactor types used for FTS; Slurry and fixed-bed tubular reactors. The different designs cause the distribution of sulphur and concentration profiles throughout the catalyst bed to be different. Thus, strategies for dealing with sulphur contaminations may be system dependent. It was recently suggested [15] to use Zn as a scavenger for sulphur in the entrance section of fixed-bed reactors due to its ability to form ZnS. Manganese is another compound known for its ability to absorb sulphur [17, 18], thus potentially guarding the FTS activity.

Manganese is also a well-known promotor for CO hydrogenation via FTS to olefins [19], with demonstrated effects on Fe, Ru and Co based catalysts, and perhaps mostly forgotten, also on the early Ni based catalysts investigated during the 1930s [2]. Un-supported oxidized Co-Mn catalysts generally consists of mixed cobalt manganese spinels $(CoMn)_3O_4$, where the ratio of Co/Mn in the spinel depends on composition and pre-treatment [20-23]. In general, Mn loading has a significant effect on water-gas-shift activity, increasing with Mn content, but increasing the pressure exerts a negative effect [21, 22]. The effect on hydrocarbon selectivity has been the main motivation for modifying with Mn, due to its ability to promote light olefin formation, particularly the valuable C_2-C_4 olefins that are otherwise are obtained by cracking of light alkanes and naphtha. Suppressing methane formation at moderate reaction conditions is another key feature of Co-Mn catalysts [24-26]. For supported catalysts, it has been demonstrated by STEM-EELS and EXAFS that the extent of interaction between Mn and Co largely determines the enhancement of selectivity [27, 28]. This enhanced selectivity has been attributed to structural and electronic effects effectively suppressing hydrogenation activity [29]. As a final note, scaling up and ensuring proper attrition strength is significant for industrial application, but variables such as binder composition and compression pressure for pelletizing affects the final selectivity for Co-Mn catalysts [30].

Due to the above-mentioned properties, the effect of sulphur on a Co-Mn catalyst cannot readily be established without extensive testing, and to our knowledge no previous reports exists detailing industrially relevant long-term effects. The following study involved long term fixed-bed testing at 5 bar and 240 °C using syngas ($H_2/CO = 2$) contaminated with 15 ppb – 10 ppm H_2S, and characterization of fresh and spent catalysts to better understand the effect of sulphur.

2 Experimental

2.1 Catalyst preparation and testing

Co-Mn catalysts were prepared by controlled precipitation from aqueous solutions of nitrate precursors at 80 °C under continuous stirring while maintaining pH 7. The precipitate was filtered and washed several times with warm distilled water, followed by drying at 120 °C for 10-18 h and calcination in static air at 400-600 °C for 15-24 h, as described in patents [31, 32]. The conditions for catalyst testing were 240 °C, 5 bar and $H_2/CO = 2.1$. Nitrogen (3%)

served as an internal standard for quantification. A 10 mm ID steel tube fixed-bed reactor was loaded with 1 g catalyst mixed with 6 g inert SiC. The reactor system, illustrated in Figure 1, was pressurized with He for leak testing and H_2/N_2 = 1/1 (140 Nml/min) was introduced at ambient pressure. The sample was heated at 3 °C/min to the reduction temperature of 350 °C, and held for 16 h. After reduction, the sample was cooled to 230 °C and the reactor was pressurized with He (250 Nml/min) to 5 bar before introducing syngas at a constant feed rate of 40 Nml/min; this corresponds to a weight hourly space velocity of ~2400 (Nml/g_{cat}·h). The temperature in the catalyst bed was then slowly increased up to 240 °C. Downstream of the catalyst bed products were fed via a heated line (160-170 °C) into a HP 6890 gas chromatograph equipped with Porapak Q + carbosieve packed columns, GS-Alumina PLOT column, a thermal conductivity detector (TCD) and a flame ionization detector (FID). A hot trap (~90 °C) collected wax and heavy condensate products while a cold trap (~25 °C) placed downstream collected water and light condensate. Hot and cold traps also collected products after the GC. At the end of the test, syngas was replaced with H_2 (150 Nml/min) for 2 hours followed by N_2 (150 Nml/min) for 5 hours, both at 260 °C. After cooling to 35 °C, passivation was performed in 0.5% O_2/N_2 (150 Nml/min) for 2 hours, and the catalyst was unloaded.

2.2 Catalyst characterization

The overall bulk composition of the catalyst was analysed using X-ray fluorescence (XRF). The sample was prepared by thorough mixing 0.2 g catalyst with 2.8 g boric acid in a mortar followed by pressing to a disc of 40 mm diameter. A standard commercial unit (Rigaku Supermini 200) was used at normal sampling intervals together with fixed-angle measurements for collecting characteristic wavelengths of known elements. Composition analysis was carried out based on phase identifications obtained by powder X-ray diffraction. The elemental analysis was extended and complimented by high-resolution inductively coupled plasma mass spectrometry (HR-ICP-MS), Thermo Electronic Corp., Waltham, MA) at the Department of Chemistry, Norwegian University of Science and Technology (NTNU).. Before HR-ICP-MS analysis the samples were decomposed with HNO_3 in an UltraClave and the resultant solution was diluted.

Prior to characterization of spent catalysts, the sample was refluxed with 250 ml xylene in a soxhlet extraction apparatus for 48 h to remove wax. The sample was removed from the apparatus and xylene evaporated overnight in a fume hood before the sample was vacuum dried at room temperature overnight. The sample was then suspended in iso-propanol and further separation was performed by ultrasonication and sedimentation of SiC.

For powder XRD analysis, a small amount of catalyst was suspended in iso-propanol and dried on a Si single crystal sample holder. Data were collected using a Bruker D8 Advance A25 powder diffractometer equipped with a Cu Kα radiation source and Lynxeye XE™ detector, with phases identified via reference to the ICCD PDF4+ database. Rietveld type analysis was performed using the Bruker Topas software package, v5 to confirm the phases identified from the PDF4+ database.

The surface chemistry was investigated with XPS on a Kratos Analytical Axis Ultra^{DLD} using monochromatic Al Kα radiation. Low energy electrons were used for charge neutralisation and the energy scale of the spectra were referenced based on the C 1s peak of alkyl bonds from adventitious carbon, set to 284.8 eV binding energy (BE). CasaXPS software was used for peak fitting and composition analysis.

The nanostructure of particles and their composition were studied using TEM and scanning TEM (STEM), with EDS for X-ray composition analysis, complimented by electron energy loss spectroscopy (EELS). A small quantity of catalyst suspended in isopropanol that was dropped into a clean agate mortar and the suspension was crushed. The crushed suspension was placed on a carbon support film on a Cu mesh supported grid and dried. The dried grid was then examined directly using a JEOL 2100F instrument equipped with an Oxford Instruments EDS system, and a JEOM ARM200 with a JEOL Centurio EDS system.

3 Results and discussion

3.1 Measurements of catalytic activity and selectivity

Activity and selectivity data were obtained as a function of time on stream (TOS). The effect of sulphur on the relative activity, normalized to 250 h TOS, is illustrated in Figures 2a and 2b. When introducing sulphur after ~300 h TOS a dose dependent effect was observed. The relative initial effect of up to 10 ppm H_2S was calculated based on the activity curve and illustrated in Figure 2c. It is worth noting that neither the activity nor the selectivity was fully

stabilized in a long-term perspective (> 1000 h) at the point when sulphur was introduced after ~300 h. At these conditions, gradual changes in selectivity was typically observed during the first 1000 h TOS with the CO_2 selectivity from water-gas-shift slowly reaching steady-state, as illustrated in Figure 2d. The CO_2 selectivity was also not entirely stable and there appeared to be local changes occurring that affected water-gas-shift activity during these long tests, for example as shown by the sudden changes observable after > 1250 h TOS and after > 2500 h TOS (Figure 2d). The activity typically reached a semi-stable state after 200-500 h in the absence of sulphur. This needs to be considered when interpreting the effect of sulphur dosed after ~300 h TOS, also as compared to dosing sulphur after ~1000 h TOS. Figure 2c illustrates that the loss in activity (% / 100 h) was significantly higher when dosing 1 ppm after ~1000 h TOS compared to after ~300 h TOS. Again, it should be noted that the activity had not reached its potential maximum after ~300 h, and as illustrated in Figure 2b, the rate of deactivation in both tests with 1 ppm H_2S approached the same level after > 1250 h TOS. Still, the results illustrate a comparably stronger effect of sulphur breakthrough from upstream processes reaching the catalyst after ~1000 h as compared to after ~300 h. This is a significant result with respect to operational risks.

With the expectation that Mn can act as a sorbent for sulphur, it is interesting to compare the rate of deactivation with other studies. Converting the values from Borg et al. [3], their reported initial rate of deactivation at 20 bar, 483 K and $H_2/CO = 2$ was a loss of 0.58 % / h at 2.5 ppm H_2S. This is > 10 times the rate predicted at 2.5 ppm H_2S from Figure 2c for the Co-Mn catalyst with sulphur dosed after ~300 h. Although the conditions are significantly different with respect to pressure and temperature, it is reasonable to assume that the presence of Mn to some extent protects the catalytic activity in the presence of sulphur, likely by absorbing or reacting with sulphur. This is further discussed in the characterization section below.

At 170 °C and 5 bar, using flash calculations in ASPEN HYSYS, it was estimated that > 99.9 % of CH_4, > 99 % of C_2-C_4, > 98 % of C_5-C_6 and > 95 % of C_7-C_8 hydrocarbons would be in the gas phase. Thus, online measurements yielded a satisfying carbon balance for C_1-C_6(C_8) compounds. For C_{9+} hydrocarbons > 10% would condense at these conditions and were therefore omitted from online analysis. In Figures 3a and b, the product distribution of C_1-C_6 olefins and paraffins are illustrated before and after introducing 5 ppm H_2S after ~300 h TOS. The main effect was a small loss in C_1-C_3 selectivity for both paraffins and olefins when comparing results with and without sulphur at the same conversion level, with a corresponding increase in C_{4+} selectivity. The H_2/CO feed usage ratio was observed to change from about 1.71 to 1.69 upon introducing 5 ppm sulphur, which corresponded to a slight increase in olefin/paraffin ratios for C_{4+} components.

Where 1 ppm H_2S was introduced after ~1000 h TOS, larger effects on selectivity were observed. However, the interpretation is difficult due to a simultaneous burst in CO_2 selectivity. The difficulty arises from a comparable boost in CO_2 selectivity and changes to hydrocarbon selectivity observed during long term steady-state operation with 15 ppb H_2S (Figure 2d). The 15 ppb H_2S was introduced after ~300 h, while the changes in selectivity occurred after > 1250 h TOS and > 2500 h TOS. In effect, with changes in water-gas-shift activity the olefin/paraffin ratios dropped significantly, likely due to increased hydrogenation activity (Figure 3c). A significant shift was seen in the 1-olefin to total olefins ratio, and 2-olefin/1-olefin ratio for C_4-C_8, as illustrated in Figure 3e. Thus, both branching and hydrogen transfer reactions were affected, but since the same effect was observed during steady-state operation with 15 ppm H_2S, it cannot be concluded that the changes were directly due to sulphur in the case where 1 ppm H_2S was introduced after ~1000 h TOS, even though the sudden changes coincided. It must also be emphasized that this strong effect on olefin composition was not observed in any of the tests where sulphur was introduced after ~300 h TOS, as illustrated in Figure 3d and f where 5 or 10 ppm H_2S was introduced, respectively. It is more likely that the changes in selectivity are linked to changes affecting the water-gas-shift reaction, which subsequently impacts the hydrocarbon selectivity. Since Mn is important for the shift activity it is plausible that sulphur reacting with Mn may indirectly impact the selectivity through changes in shift activity, but we have no clear strong evidence that it has a direct mechanistic effect related to the hydrocarbon formation.

3.2 Characterization of samples

Elemental analysis by XRF and HR-ICP-MS indicated that the bulk Co/Mn ratio was close to one. Traces of Ni (< 1000 ppm) and Fe (< 500 ppm), probably associated with the precursors used for Mn and Co were also present. Small traces of Mg (< 15 ppm) and Ca (< 100 ppm) were identified by HR-ICP-MS, while a significant amount of Na (1000-2000 ppm) was detected.

In Figure 4 several diffractograms are shown for spent catalysts. There is a progression from bottom to top for the spent samples with respect to increasing time on stream. Sample (a) illustrate a catalyst tested for 294 h TOS without H_2S, and samples (c)-(d) are spent catalysts tested for 1356 h and 2135 h TOS, respectively, both exposed to 1 ppm H_2S in the feed. Sample (b) is a spent catalyst tested for > 1000 h with 10 ppm H_2S in the feed, but this sample was reduced-oxidized-reduced (ROR) twice with testing both in-between and after attempting to regenerate the activity. The ROR cycle did not improve or recover the activity. The diffractograms are compared with powder diffraction references, and the Rietveld analysis of sample (c) after 1356 h TOS, including 1000 h with 1 ppm H_2S, is also shown. The separation of the catalyst from SiC after activity testing was largely successful. A cubic (Mn, Co)O phase is present with peaks at ~35.6 °, ~41.4 ° and ~60.0 ° 2θ, and exhibits broad diffraction peaks due to a likely combination of small crystallite size and compositional inhomogeneity. The observed unit cell parameter is consistent with a Mn-rich composition of approximately $Mn_{2/3}Co_{1/3}O$. For samples (c) and (d) weak diffraction lines corresponding to pure MnO are also observed. This can be explained by the reduction and transport of Co out of the mixed oxide phase during long term exposure to syngas to form metallic Co nanoparticles and clusters thereof, leaving behind a pure MnO phase. Peaks corresponding to the hexagonal polymorph of Co pattern confirm the presence of such Co nanoparticles, as observed with TEM (see Figures 7 and 8). Unfitted intensity in the region of 44.3° 2θ accords with the presence of the cubic polymorph of Co, but other peaks for this phase are absent. It may then indicate some cubic-type stacking disorder, but this cannot be conclusively confirmed from the data. An interesting feature possibly linked to non-sulphur related deactivation is several peaks, most distinct at ~42.5 ° and ~45.8 °, which correspond to presence of Co_2C. The absence of this phase on sample (b) is possibly linked to the ROR procedure carried out in attempt to regenerate the sample.

The surface compositions of fresh and spent samples were measured by using XPS. Figure 5 illustrates survey scans of the fresh sample, confirming the presence of Na, as well as the sample tested for > 1000 h TOS with 10 ppm H_2S, followed by two attempts to regenerate by ROR (from Figure 1a, data after ROR is not shown) Total exposure levels of H_2S for each of these tests are shown in Table 1. There is a noteworthy difference in Co/Mn ratio between the fresh and spent samples (Table 1). The lower Co/Mn ratio in spent samples can be explained by formation of large Co nanoparticles, as migration of Co out of the mixed Co-Mn oxide to form nanoparticles would increase the relative XPS signal from Mn. A similar mechanism has been proposed before, involving migration of Co^{2+} ions to the reduction front [23]. The oxidation state for the spent samples was likely affected by the passivation procedure, soxhlet extraction and general exposure to air, and is therefore comparable to the fresh sample.

The C 1s peaks could be fitted using reference energies and GL(30) peaks, as detailed in Table 2. The binding energies shown below the table are the ranges used for fitting. The full width at half maximum (FWHM) was locked for all oxygen containing species relative to C-OH/C-O-C.. The fresh sample exhibited C 1s peaks typical for adventitious carbon, dominated by aliphatic species with minor contributions from species with single and double oxygen bonds. The spent sample, illustrated in Figure 6a, was found to show signal corresponding to a carbide species. This is likely Co_2C as SiC was not detected in the XRD spectrum of this sample. Some oxygen-containing carbon species were also present on the spent sample and there was some indication that carbonates as well as poly-aromatics/organic acids/esters, likely products from the FTO synthesis, could be present, even after soxhlet extraction to remove the wax.

According to Biesinger [33] the Co $2p_{3/2}$ peak for CoO can be fitted with two main GL(30) peaks at 780-782 eV BE together with a satellite feature at 786-787 eV BE. However, there are no reference spectra suitable for evaluating mixed Co-Mn oxides. Nevertheless, fitting was attempted using both the Co $2p_{3/2}$ and Co $2p_{1/2}$ peaks and their satellites simultaneously, as illustrated in Figure 6b. The overall electronic structure resemble that of $CoO/Co(OH)_2$ more than that of Co_3O_4 [33]. There was no clear indication of a metallic feature at ~778 eV BE in any of the samples. This is to be expected, as the fresh catalyst had been calcined and the spent sample had been passivated with 0.5% O_2 before being removed from the reactor, exposed to air and rinsed with xylene. The Mn 3s spectra in Figure 6c were used to assess the oxidation state of Mn by looking at the peak splitting [34, 35]: MnO (Mn^{2+}) 5.7-6.2 eV, Mn_2O_3 (Mn^{3+}) 4.6-5.4 eV (4.6 for MnOOH, Mn_2O_3 typically 5.2-5.4 eV), MnO_2 (Mn^{4+}) 4.5-4.7 eV. Thus, Mn appears to be predominantly Mn^{2+} on the surface of the fresh and spent catalysts after exposure to air. This agrees well with the observation of (CoMn)O phases in the samples by XRD.

HR-ICP-MS analysis of sulphur content on spent catalyst samples is also shown in Table 1. Comparing the wt% measured by HR-ICP-MS and the amount of sulphur fed to the system (calculated from TOS feed concentration), it may be concluded that all sulphur fed to the system was deposited on or reacted with the catalyst to form sulphates, sulphides or sulphurous deposits. The total amounts (125, 343 and 561) measured in µmol/g were significantly larger than the fresh cobalt surface area measured by H_2 chemisorption (90 µmol H/g.Strong local concentrations of sulphur were evidenced by TEM, as described below. The S 2p spectrum of the spent sample exposed to 10 ppm H_2S was modelled using reference energies [36, 37] as illustrated in Figure 6d, in order to estimate the quantity of different phases. The $2p_{3/2} – 2p_{1/2}$ split was fixed to 1.15 eV and the ratio for the doublets was constrained to 2:1. Considering the observation of strong local concentrations of sulphur and the position of different S 2p reference peaks [36, 37], organically bound sulphur cannot be ruled out, and the relative ratio of different species could be different in other parts of the sample or *in situ* during the Fischer-Tropsch reactions.

STEM/EDS of a spent ultra-microtomed sample is illustrated in Figure 7, and STEM/EDS of the sample after suspension and crushing is shown at high magnification in Figure 8. These two figures give a good impression of the catalyst particle morphology and composition after testing. Comparison of the Mn and Co maps in Figure 7 shows the overall distribution of (Mn,Co)O. The Co map suggest that the larger Co particles have formed between the (Mn,Co)O aggregates, and examples of this are marked with arrows in Figure 7. This shows the benefit of ultramicrotomy preparation. Several discrete regions enriched in S are seen in the S map. Comparison of the STEM image and EDS maps in Figure 8 shows that most of the material in the field of view is (Mn,Co)O, with a crystallite size of a few tens of nanometres, along with a distribution of discrete Co particles. One of the Co particles, which could be a dense aggregate of particles at the centre of the field of view, has a diameter of 60-80 nm, while smaller Co particle are seen present around. The metallic Co particles showed surface oxidation, attributed to passivation and exposure to air. Different regions in Figure 8 are marked with numbers and the EDS spectra of regions 1-3 are illustrated in Figure 9. The EDS spectrum 1 is from a region showing finer (Mn,Co)O crystallites. Spectrum 2 was obtained from the large Co particle near the centre of the field of view. This also shows a small S signal, again possibly confirming the presence of S on the Co nanoparticle(s) in accordance with the notion of site titration. Spectrum 3 was obtained from the S-rich region. The latter shows a strong correlation of S with Mn, relative to Co. A strong O signal was also present in this region (not illustrated). This is consistent with the presence of the sulphate suggested by XPS. Figure 10 shows Electron Energy Loss Spectroscopy (EELS) analysis from a different position in the same specimen. The spectra show the energy range that includes O, Mn and Co edges. The lower spectrum was obtained from a region of mixed oxide where peaks for all three elements are present. The upper spectrum was obtained from a metallic Co particle. The latter shows very weak O and Mn, peaks which may be attributed to a thin surface oxide layer and limited overlap with the oxide catalyst-phase. The spectrum is consistent with the presence of pure metallic Co in the spent catalyst.

4 Conclusions

The effects of H_2S on a Co-Mn FTO catalyst depended on when H_2S was introduced. Starting dosing of sulphur after ~1000 h TOS had a significantly larger negative effect than dosing it after ~300 h. When dosing after ~300 h the initial loss in activity correlated linearly to the concentration of H_2S in the feed. The main effect of H_2S was titration of sites responsible for the rate limiting step. The effect on selectivity was more complex due to changes in shift activity. There was no clear effect on shift activity or hydrocarbon selectivity when dosing after ~300 h, while dosing after ~1000 h TOS the introduction of sulphur coincided with changes in shift activity and hydrocarbon selectivity. However, boosted shift activity and changes in hydrocarbon selectivity was also observed after long time testing at steady-state with 15 ppm H_2S, leading to the conclusion that sulphur may react with Mn and thereby have an effect of shift activity, which again impacts hydrocarbon selectivity. The effect of H_2S on activity was substantially less than for a conventional Co FTS catalyst, likely due to Mn acting as a sacrificial element reacting with H_2S to form a sulphurous species. After removing the catalyst from the reactor, following passivation and the subsequent *ex situ* wax extraction these sulphurous species were mainly $MnSO_4$. In addition to the effect of sulphur on the long-term activity and selectivity, both were also likely affected by sintering and carbide formation. A wide range of particle sizes and aggregates were observed with TEM after testing, ranging up to 60-80 nm, and Co_2C was identified from both XRD and XPS analysis of the spent sample.

References

[1] Anderson RB, The Fischer-Tropsch Synthesis, Academic Press Inc., Orlando, 1984.
[2] Storch HH, Golumbic N, Anderson RB, The Fischer-Tropsch and Related Syntheses, Wiley, New York, 1951.
[3] Borg Ø, Hammer N, Enger BC, Myrstad R, Lindvåg OA, Eri S, Skagseth TH, Rytter E (2011) J. Catal. 279:163.
[4] Bartholomew CH, Bowman RM (1985) Applied Catalysis 15:59.
[5] Curtis V, Nicolaides CP, Coville NJ, Hildebrandt D, Glasser D (1999) Catal. Today 49:33.
[6] Li J, Coville NJ (2001) Appl. Catal. A 208:177.
[7] Visconti CG, Lietti L, Forzatti P, Zennaro R (2007) Appl. Catal. A 330:49.
[8] Madikizela-Mnqanqeni NN, Coville NJ (2008) Appl. Catal. A 340:7.
[9] Pansare SS, Allison JD (2010) Appl. Catal. A 387:224.
[10] Visconti CG, Lietti L, Tronconi E, Forzatti P, Zennaro R, Rossini S (2010) Catal. Today 154:202.
[11] Sparks DE, Jacobs G, Gnanamani MK, Pendyala VRR, Ma WP, Kang J, Shafer WD, Keogh RA, Graham UM, Gao P, Davis BH (2013) Catal. Today 215:67.
[12] Bambal AS, Guggilla VS, Kugler EL, Gardner TH, Dadyburjor DB (2014) Ind. Eng. Chem. Res. 53:5846.
[13] Ehrensperger M, Wintterlin J (2015) J. Catal. 329:49.
[14] Barrientos J, Montes V, Boutonnet M, Jaras S (2016) Catal. Today 275:119.
[15] Liu ZX, Wu DP, Xing Y, Guo XH, Fang SM (2016) Appl. Catal. A 514:164.
[16] Ma WP, Jacobs G, Shafer WD, Pendyala VRR, Xiao QF, Hu YF, Davis BH (2016) Catal. Lett. 146:1204.
[17] Guo LF, Pan KL, Lee HM, Chang MB (2015) Ind. Eng. Chem. Res. 54:11040.
[18] Chytil S, Kure M, Lodeng R, Blekkan EA (2015) Fuel Process. Technol. 133:183.
[19] Galvis HMT, De Jong KP (2013) Acs Catal 3:2130.
[20] Liang Q, Chen KD, Hou WH, Yan QJ (1998) Appl. Catal. A 166:191.
[21] Keyser MJ, Everson RC, Espinoza RL (1998) Appl. Catal. A 171:99.
[22] Keyser MJ, Everson RC, Espinoza RL (2000) Ind. Eng. Chem. Res. 39:48.
[23] Guse K, Papp H (1993) Fresenius Journal of Analytical Chemistry 346:84.
[24] Hutchings GJ, Copperthwaite RG, Vanderriet M (1995) Top. Catal. 2:163.
[25] Johns M, Landon P, Alderson T, Hutchings GJ (2001) Chem. Commun. (Cambridge, U. K.) 2454.
[26] Zhang JL, Ren J, Chen JG, Sun YH (2002) Acta Phys-Chim Sin 18:260.
[27] Morales F, Grandjean D, De Groot FMF, Stephan O, Weckhuysen BM (2005) Phys. Chem. Chem. Phys. 7:568.
[28] Bezemer GL, Radstake PB, Falke U, Oosterbeek H, Kuipers H, Van Dillen A, De Jong KP (2006) J. Catal. 237:152.
[29] Morales F, De Smit E, De Groot FMF, Visser T, Weckhuysen BM (2007) J. Catal. 246:91.
[30] Zakeri M, Samimi A, Khorram M, Atashi H, Mirzaei A (2010) Powder Technol. 200:164.
[31] Karim K, Khan AA, Rakib MA, Al-Semahi M, Barochia J, US2016/0175819 A1.
[32] Karim K, Rakib MA, Khan AA, Al-Semahi M, US 2016/0167025 A1.
[33] Biesinger MC, Payne BP, Grosvenor AP, Lau LWM, Gerson AR, Smart RSC (2011) Appl. Surf. Sci. 257:2717.
[34] Cerrato JM, Hochella MF, Knocke WR, Dietrich AM, Cromer TF (2010) Environmental Science & Technology 44:5881.
[35] Junta JL, Hochella Jr MF (1994) Geochimica et Cosmochimica Acta 58:4985.
[36] Naumkin AV, Kraut-Vass A, Gaarenstroom SW, Powell CJ, NIST Standard Reference Database 20, Version 4.1 (web version), 2012.
[37] Biesinger MC, X-ray Photoelectron Spectroscopy (XPS) Reference Pages, 2015.
[38] Wesner DA, Linden G, Bonzel HP (1986) Appl. Surf. Sci. 26:335.
[39] Sasaki S, Fujino K, Takeuchi Y, Sadanaga R (1980) Acta Crystallographica Section A 36:904.

Table 1 XPS elemental surface composition of fresh, *ex situ* reduced (exposed to air) and spent catalyst samples exposed to sulphur during testing. HR-ICP-MS analysis of sulphur in spent catalyst samples exposed to sulphur during catalyst testing.

Table 2 Comparison of deconvolution of C 1s spectra for fresh and spent catalyst.

Table 1

	XPS		HR-ICP-MS		Sulphur feed
Sample	Co/Mn	M^{+x}	S [wt %]	S [µmol/g]	TOS*Feed conc. S [wt %]
Fresh	1.67	1.96	24 ppm	< 1	-
553 h at 10 ppm H_2S	0.58	1.62	1.8	561	1.9
629 h at 5 ppm H_2S	0.75	1.42	1.1	343	1.1
1040 h at 1 ppm H_2S	0.56	1.95	0.4	125	0.4

M: metals, M^{+x}: estimated metal oxidation state from (O-Na-4*S)/(Co+Mn)

Table 2

Sample	Carbide [at %]	CO/Co [at%]	C-C, C-H [at %]	C-OH, C-O-C [at %]	C=O [at %]	O-C=O [at%]	Carbonate [at%]	Poly-aromatics, organic acids, esters [at %]
Fresh	-	-	65.8	21.0	-	13.2	-	-
Spent	2.5	-	76.5	6.4	1.4	10.1	2.3	0.8

Inorganic carbide: 282-282.6 eV BE, CO/Co: 283.4 eV BE [38], C-C, C-H: 284.8, 285.2 eV BE, C-OH, C-O-C: 286-286.2 eV BE, C=O: 287.1-288.3 eV BE, O-C=O: 288.6-289 eV BE, Carbonate: 289.8 eV BE, poly-aromatics, organic acids, esters: 291.6 eV BE.

Figure 1 Schematic illustration of the experimental unit used for catalyst testing.

Figure 2 a) Relative activity as a function of time on stream, normalized to 250 h TOS, illustrating tests where 15-30 ppb (dark blue), 5 ppm (medium blue) and 10 ppm H_2S (light blue) were continuously dosed from ~300 h TOS. b) Relative activity as a function of time on stream, normalized to 250 h TOS, illustrating two tests where 1 ppm H_2S was continuously dosed from ~300 h or ~1000 h TOS. c) Relative initial effect on activity measured in % loss / h vs dosing levels of H_2S after ~300 h (blue and green dots) and after ~1000 h (red dot) TOS. d) Selectivity to CH_4 and CO_2 as functions of time on stream for the test with 0-30 ppb H_2S, dosed as illustrated in a).

Figure 3 Product distribution of olefins and paraffins using the average of samples collected from the same run before and after introduction H_2S (average CO conversion in both cases was 51.4%): a) between 260-290 h TOS in the absence of sulphur and b) between 385-425 h TOS in the presence of 5 ppm H_2S. c and e) illustrating the effect of a sudden change in water-gas-shift activity largely coinciding with feeding 1 ppm H_2S after ~1000 h TOS, with changed shift activity impacting 1-olefin/total olefins and 2-olefin/1-olefin ratios. d and f) illustrating comparably no effect on selectivity from 10 ppm H_2S without concurrent changes in shift activity.

Figure 4 Left: Zoomed region of the XRD spectra for: a) spent catalyst tested for 294 h TOS without sulphur, b) spent catalyst tested for > 1000 h TOS with 10 ppm H_2S from 306-859 h TOS followed by two attempts to regenerate with reduction-oxidation-reduction, c) spent catalyst tested for 1356 h TOS with 1 ppm H_2S from 316-1356 h TOS, d) spent catalyst tested for 2135 h TOS with 1 ppm H_2S from 1000-1842 h TOS. Product phases identified are the hexagonal polymorph of Co (PDF 04-001-3273), MnO [39] (PDF 04-005-4310) and Co_2C (PDF 04-004-4639). Right: Zoomed portion of Rietveld-type analysis of XRD data from plot c).

Figure 5 XPS survey spectra of fresh and *ex situ* reduced (exposed to air) and spent catalyst (from testing with 10 ppm H_2S).

Figure 6 XPS spectra of fresh and spent catalyst (from testing with 10 ppm H_2S), showing; a) C 1s spectra with peak fitting detailed in Table 2, b) Co 2p spectra, c) Mn 3s spectra with peak splitting, and d) S 2p spectra with peak fitting $2p_{3/2}/2p_{1/2}$ (Sulfide: 161.46/162.61 eV BE, Sulphur: 163.83/164.97 ev BE, Sulphite: 166.61/167.76 eV BE, Sulphate: 168.59/169.74 ev BE).

Figure 7 Low magnification STEM image of an ultramicrotomed section of the spent sample (from testing with 10 ppm H_2S) with EDS mapping of Mn, Co and S.

Figure 8 High magnification STEM image of an ultramicrotomed section of the spent sample (from testing with 10 ppm H_2S) with EDS mapping of Mn, Co and S.

Figure 9 EDS spectra from positions marked 1-3 in Figure 8 with Kα peaks labelled between 5 and 10 eV, unlabelled peaks are Kβ signals from Mn, Co and Cu, respectively. The Cu signal stems from the Cu grid used for mounting the sample in the TEM.

Figure 10 Electron Energy Loss Spectroscopy (EELS) from two different regions in Figure 9; upper spectrum from a metallic Co particle and lower spectrum from a region of mixed oxides.

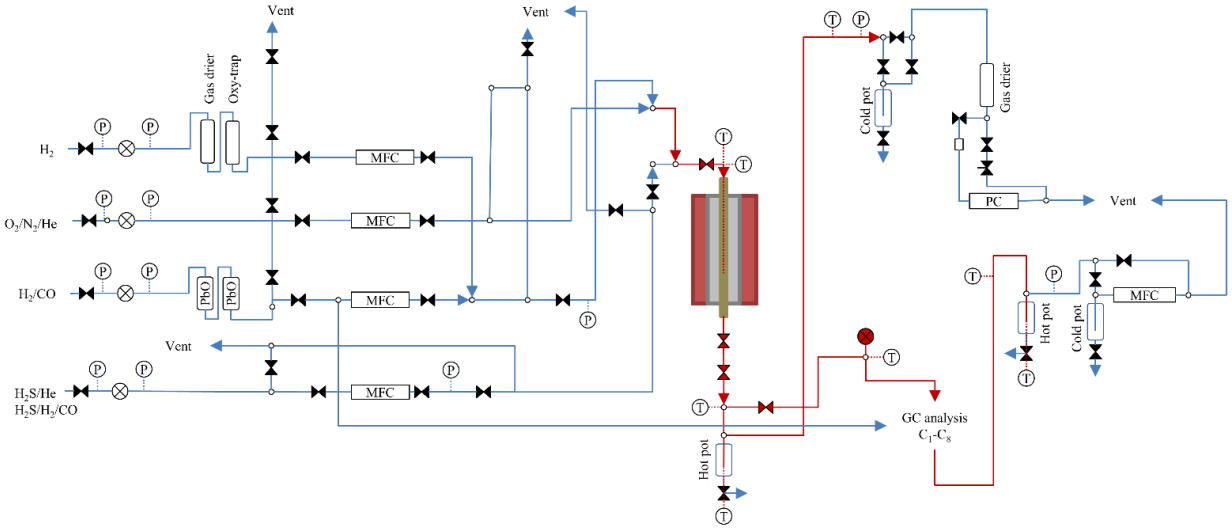

Figure 1

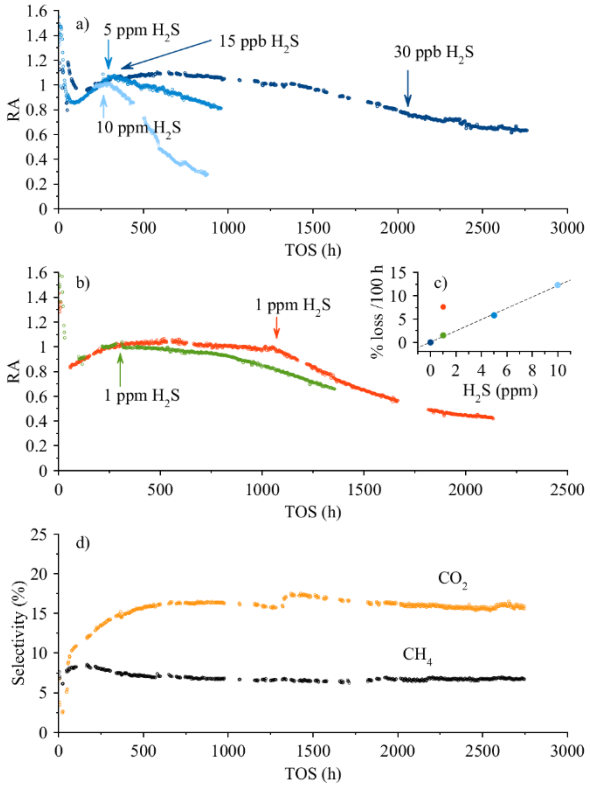

Figure 2

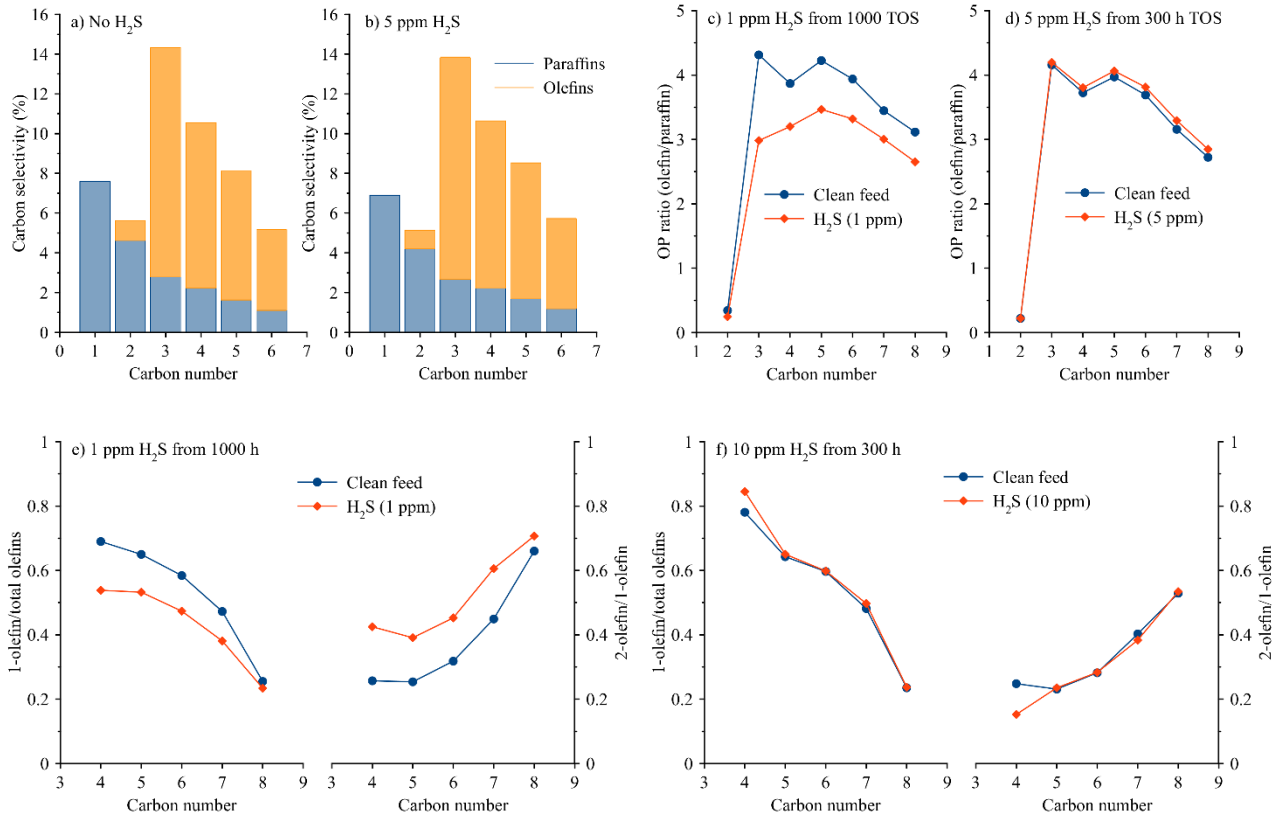

Figure 3

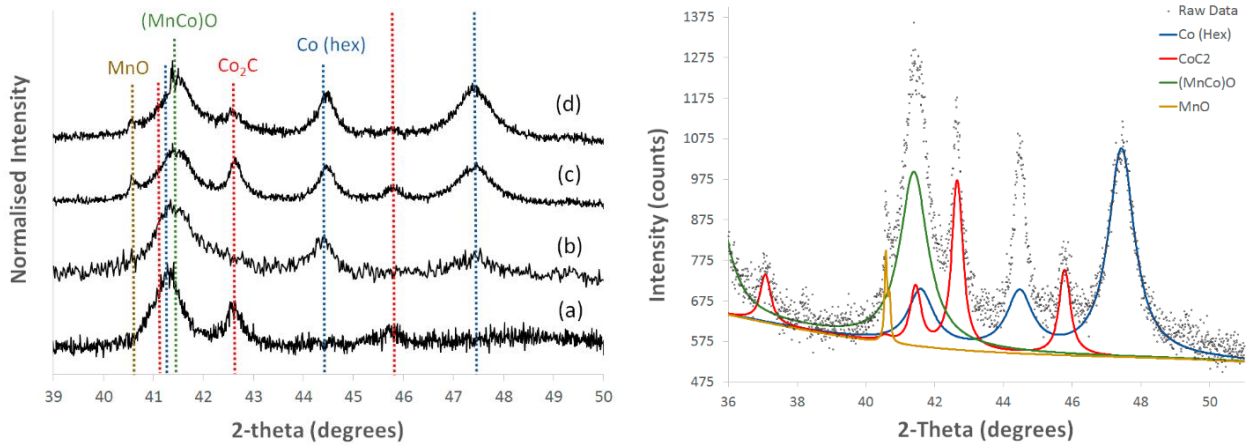

Figure 4

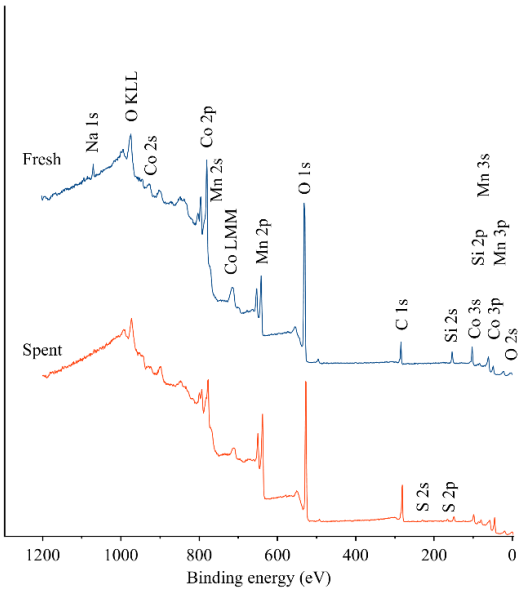

Figure 5

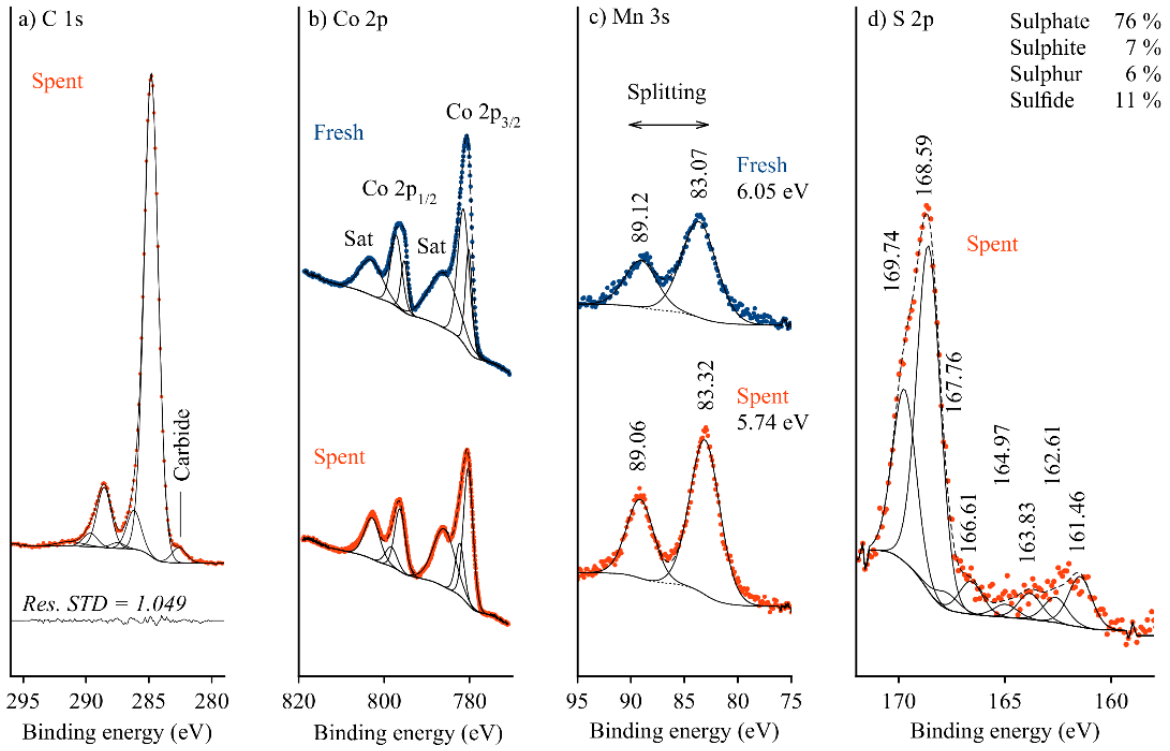

Figure 6

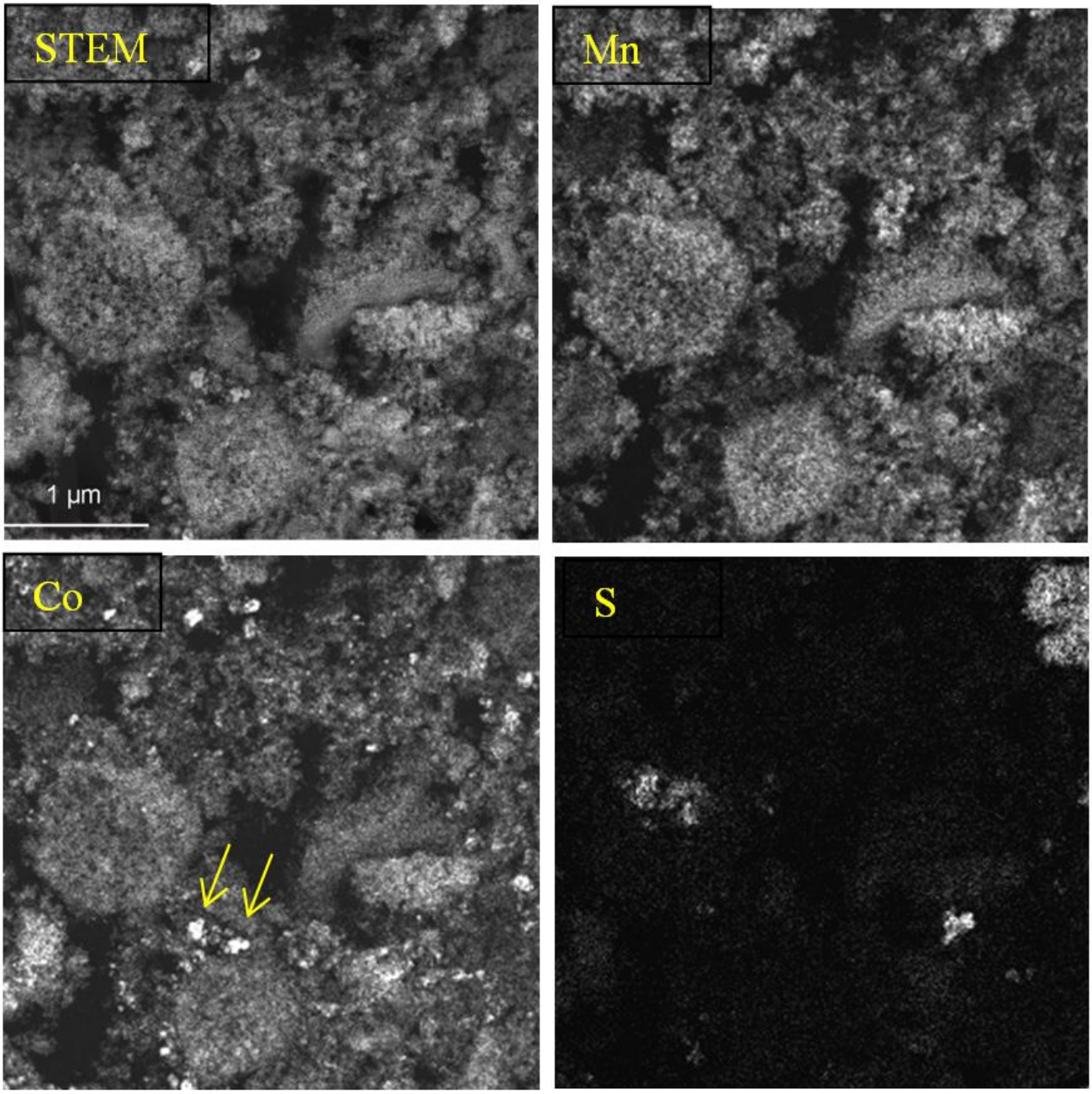

Figure 7

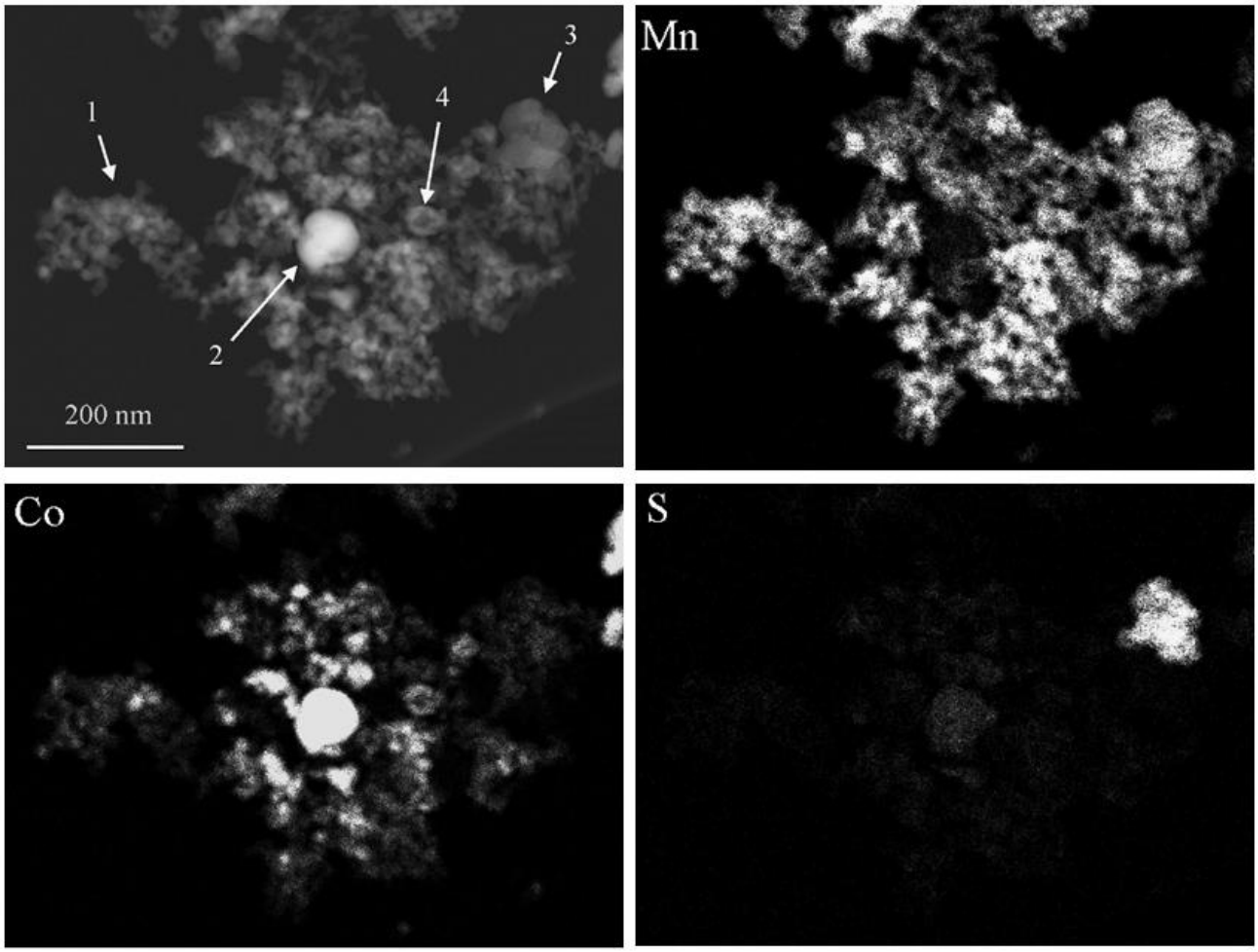

Figure 8

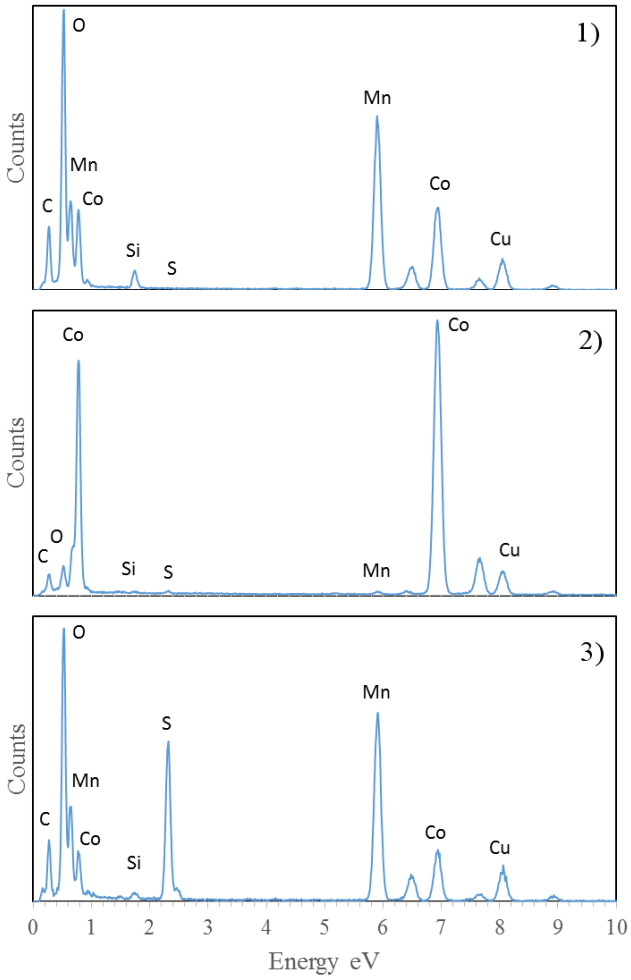

Figure 9

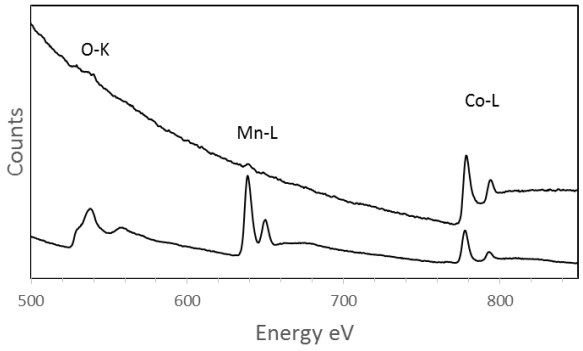

Figure 10